Crystal Growth of Organohectorite Clay As Revealed by Atomic Force Microscopy

4 AUTHORS, INCLUDING:

Kathleen A. Carrado
Argonne National Laboratory
108 PUBLICATIONS **2,109** CITATIONS

SEE PROFILE

Gerry Zajac
University of Illinois at Chicago
81 PUBLICATIONS **1,702** CITATIONS

SEE PROFILE

Crystal Growth of Organohectorite Clay As Revealed by Atomic Force Microscopy

Kathleen A. Carrado,*,† Gerry W. Zajac,‡ Kang Song,† and James R. Brenner†

Chemistry Division, Argonne National Laboratory, 9700 South Cass Avenue, Argonne, Illinois 60439, and Amoco Research Center, Amoco Corporation, P.O. Box 3011, Naperville, Illinois 60566

Noncontact atomic force microscopy, commonly referred to as "tapping mode" AFM, has been used to scan primarily the morphological features of growing hectorite clay crystallites synthesized in the presence of organoammonium cations. The use of such cations allows larger crystals to form in this system, making study by AFM feasible. This is the first time that temporal "snapshots" of a clay's nucleation and crystallization processes have been presented. The observed view does not support the perhaps predicted scene of small crystallites slowly ripening into large plates. Instead, larger aggregates appear to coalesce from numerous small crystallites that are closely associated in globular networks similar in appearance to "strings of pearls" at the initial stages of crystallization.

Introduction

Clay minerals, along with the related class of silicates called zeolites, are among one of the most important classes of heterogeneous catalysts. Their high surface areas, cation exchange capacities, and surface acidities impart high selectivities and activities in such reactions as hydrocarbon cracking. Swelling smectite clays such as montmorillonite and hectorite have attracted the most attention because of their intercalation chemistry and characteristic surface properties. Such materials swell in water, can be pillared with organic and inorganic complexes,[1] and are used as molecular sieves. There are crucial advantages to using synthetic clay minerals over natural ones, just as is done for zeolites, since materials with specific chemical compositions and crystal structures are possible. Natural smectite clays also exhibit unreliable quality in terms of lattice composition and microstructure and large variations in impurity content.

There are many scattered reports of clay synthesis in the literature. Vastly different conditions have been reported not only for different types of clays, such as montmorillonite,[2] beidellite,[3] hectorite,[4] kaolinite,[5] and mica,[6] but within the same clay type as well. As a result, no cohesive picture of clay synthesis has been put forth, and crystallization mechanisms are just beginning to be examined. For example, controlling the nucleation has been proven important for the selective synthesis of clay minerals when silicic acid is used as the silicon source.[7]

Two main routes to crystallization have been identified for zeolites, which may or may not be analogous to clays. First, single crystals could grow by transport of nutrient from the gel phase to a growing zeolite crystal, and second, gel globules could crystallize without material transport to result in globular, highly twinned crystals. The former route has been the focus of a recent atomic force microscopy (AFM) study[8] of zeolites.

AFM has been used to probe the surface features of clays[9] and zeolites[10] and also the details of crystal growth of a number of organic/biological[11] and inorganic materials.[12] Recently, the polymerization behavior of monomers on cast hectorite and montmorillonite clay thin films has been examined by AFM.[13] The present study utilizes AFM for the first time to scan primarily the morphological features of growing hectorite clay crystallites synthesized in the presence of organoammonium cations. The use of such cations allows larger crystals to form in this system,[4a] making study by AFM feasible. This is the first time that AFM has been applied to observe nucleation and growth processes of a crystalline layer silicate.

Experimental Section

Materials. A detailed procedure for the hydrothermal crystallization of an organohectorite follows. Reactants in the molar ratios of $LiF:MgO:SiO_2$ as 0.266:1.00:1.52 are refluxed for

(1) (a) Pinnavaia, T. J. *Adv. Chem. Ser.,* **1995**, *No. 245*, 283. (b) Vaughan, D. E. W. *Catal. Today* **1988**, *2*, 187.

(2) (a) Hakazawa, H.; Yamada, H.; Yoshioka, K.; Adachi, M.; Fujita, T. *Clay Sci.* **1991**, *8*, 59. (b) Yamada, H.; Yoshioka, K.; Nakazawa, H. *Miner. J.* **1991**, *15*, 300. (c) Gotoh, Y.; Okada, K.; Otsuka, N. *Clay Sci.* **1988**, *7*, 115. (d) Bailey, S. W. *Rev. Mineral.: Hydrous Phyllosilicates* **1988**, *19*, 531.

(3) Kloprogge, J. T.; van der Eerden, A. M. J.; Jansen, B. H.; Geus, J. W. *Geol. Mijnbouw* **1990**, *69*, 351.

(4) (a) Carrado, K. A.; Thiyagarajan, P.; Song, K. *Clay Miner.* **1997**, *32*, 27. (b) Barrer, R. M.; Dicks, L. W. R. *J. Chem. Soc. A.* **1967**, 1523.

(5) (a) Huertas, F. J.; Huertas, F.; Linares, J. *Appl. Clay Sci.* **1993**, *7*, 345. (b) Miyawaki, R.; Tomura, S.; Inukai, K.; Shibasaki, Y.; Okazaki, M.; Samejima, S.; Satokawa, S. *Clay Sci.* **1992**, *8*, 273. (c) Tomura, S.; Shibasaki, Y.; Miyawaki, R.; Mizuta, H.; Yamashita, Y. *Clay Sci.* **1990**, *7*, 315.

(6) (a) Paulus, W. J.; Komarneni, S.; Roy, R. *Nature* **1992**, *356*, 571. (b) Tateyama, H.; Nishimura, S.; Tsunematsu, K.; Jinnai, K.; Adachi, Y.; Kimura, M. *Clays Clay Mineral.* **1992**, *40*, 180. (c) Gregorkiewitz, M.; Rausell-Colom, J. A. *Am. Mineral.* **1987**, *72*, 515. (d) Voncken, J. H. L.; van der Eerden, A. M. J.; Jansen, J. B. H. *Am. Mineral.* **1987**, *72*, 551. (e) Rosenberg, P. E. *Am. Mineral.*, **1987**, *72*, 716.

(7) Mizutani, T.; Fukushima, Y.; Okada, A.; Kamigaito, O. *Bull. Chem. Soc. Jpn.* **1990**, *63*, 2094.

(8) Anderson, M. W.; Agger, J. R.; Thornton, J. T.; Forsyth, N. *Angew. Chem., Int. Ed. Engl.* **1996**, *35*, 1210.

(9) (a) Occelli, M. L.; Gould, S. A. C.; Drake, B. *Microp. Mater.* **1994**, *2*, 205. (b) Occelli, M. L.; Drake, B.; Gould. S. A. C. *J. Catal.* **1993**, *142*, 337. (c) Garnaes, J.; Lindgreen, H.; Hansen, P. L.; Gould, S. A. C.; Hansma, P. K. *Ultramicroscopy* **1992**, *42–44*, 1428. (d) Lindgreen, H.; Garnaes, J.; Hansen, P. L.; Besenbacher, F.; Laegsgaard, E.; Stensgaard, I.; Gould, S. A. C.; Hansma, P. K. *Am. Mineral.* **1991**, *76*, 1218. (e) Hartman, H.; Sposito, G.; Yang, A.; Manne, S.; Gould, S. A. C.; Hansma, P. K. *Clays Clay Miner.* **1990**, *38*, 337.

(10) (a) Binder, G.; Scandella, L.; Schumacher, A.; Kruse, N.; Prins, R. *Zeolites* **1996**, *16*, 2. (b) Harvey, G.; Binder, G.; Prins, R. *Stud. Surf. Sci. Catal.* **1995**, *94* (Catalysis by Microporous Materials), 397. (c) Occelli, M. L.; Gould, S. A. C.; Stucky, G. D. *Stud. Surf. Sci. Catal.* **1994**, *84* (Zeolites and Related Microporous Materials, Pt. A), 485. (d) MacDougall, J. E.; Cox, S. D.; Stucky, G. D.; Weisenhorn, A. L.; Hansma, P. K.; Wise, W. S. *Zeolites* **1991**, *11*, 429.

(11) (a) Ward, M. D.; Yip, C. M. *Biophys. J.* **1996**, *71*, 1071. (b) Rawls, R. *Chem. Eng. News* **1996**, *74* (35), 32. (c) Manne, S.; Cleveland, J. P.; Stucky, G. D.; Hansma, P. K. *J. Cryst. Growth* **1993**, *130*, 333. (d) Durbin, S. D.; Carlson, W. E. *J. Cryst. Growth* **1992**, *122*, 71.

(12) (a) Hillner, P. E.; Gratz, A. J.; Manne, S.; Hansma, P. K. *Geology* **1992**, *20*, 359. (b) Hillner, P. E.; Manne, S.; Gratz, A. J.; Hansma, P. K. *Ultramicroscopy* **1992**, *42*, 1387. (c) Gratz, A. J.; Manne, S.; Hansma, P. K. *Science* **1991**, *251*, 1343.

(13) Porter, T. L.; Eastman, M. P.; Hagerman, M. E.; Attuso, J. L.; Bain, E. D. *J. Vac. Sci. Technol., A* **1996**, *14*, 1488.
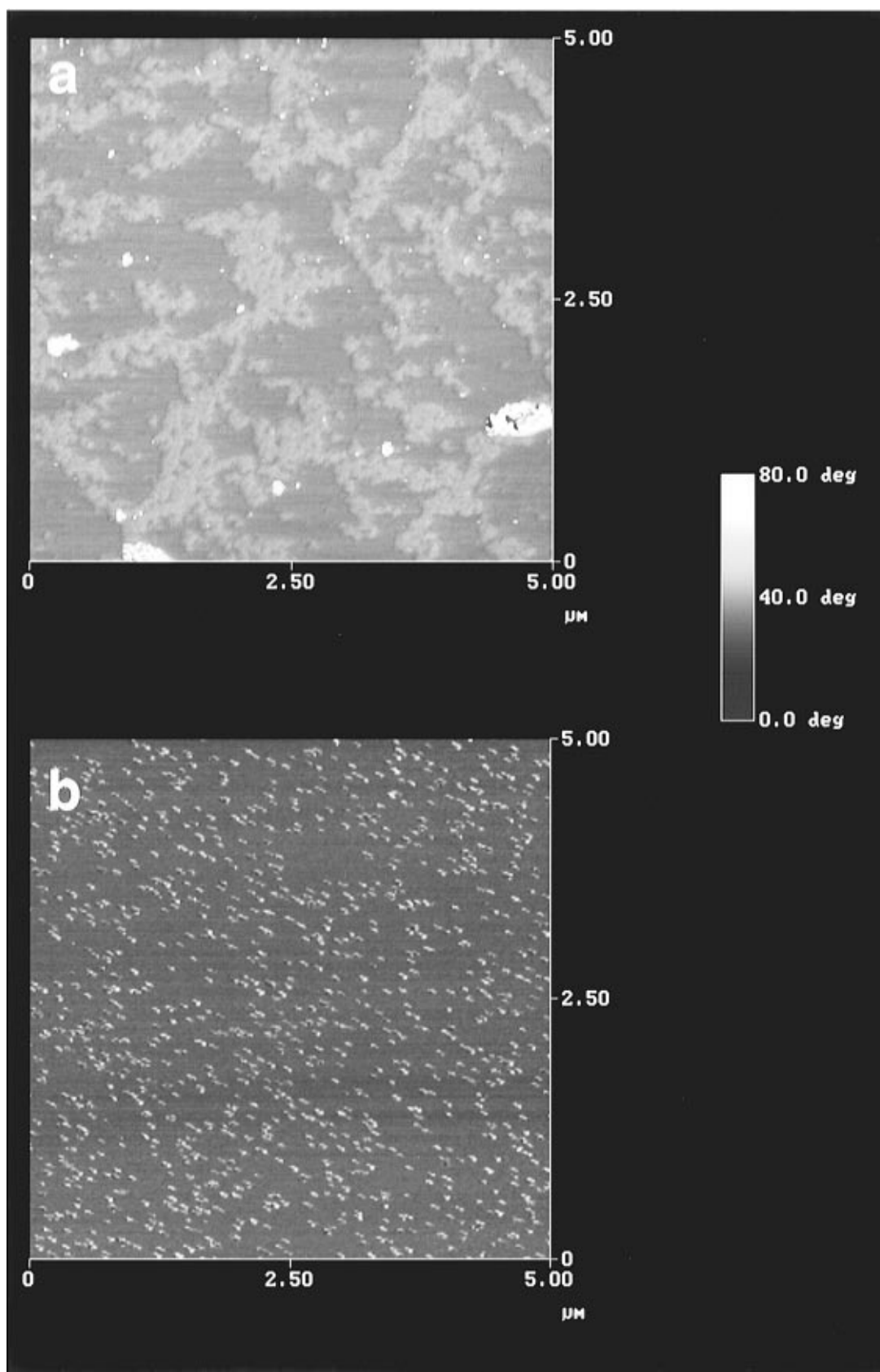
Figure 1. (a) A 5 μm TMAFM phase image of freshly prepared magnesium hydroxide (brucite); the contrast scale is 0−80°. (b) A 5 μm TMAFM phase image of colloidal silica, which consists of uniform 40−60 nm spheres; the contrast scale is 0−80°.

2 days as a 1−2 wt % aqueous slurry. This yields the ideal hectorite composition: $Ex_{0.66}[Li_{0.66}Mg_{5.34}Si_8O_{20}(OH)_4]$, where Ex is exchangeable monocation. In the purely inorganic synthetic hectorite lithium(I) is the exchangeable cation. A certain amount of this Li(I) can be replaced by organic or organometallic cations directly from a precursor organic-containing gel.[14] For mono-

cationic species, 0.066 mol is used, in which case only 0.20 mol of LiF is needed. The source of MgO was a freshly synthesized $Mg(OH)_2$ slurry. A typical scaled-down reaction begins by dissolving 2 mmol of tetraethylammonium chloride (or TEA) in water in a 1-L round-bottom flask, to which 0.16 g (6 mmol) of LiF is added with vigorous stirring. Separately, 6.5 g (0.024
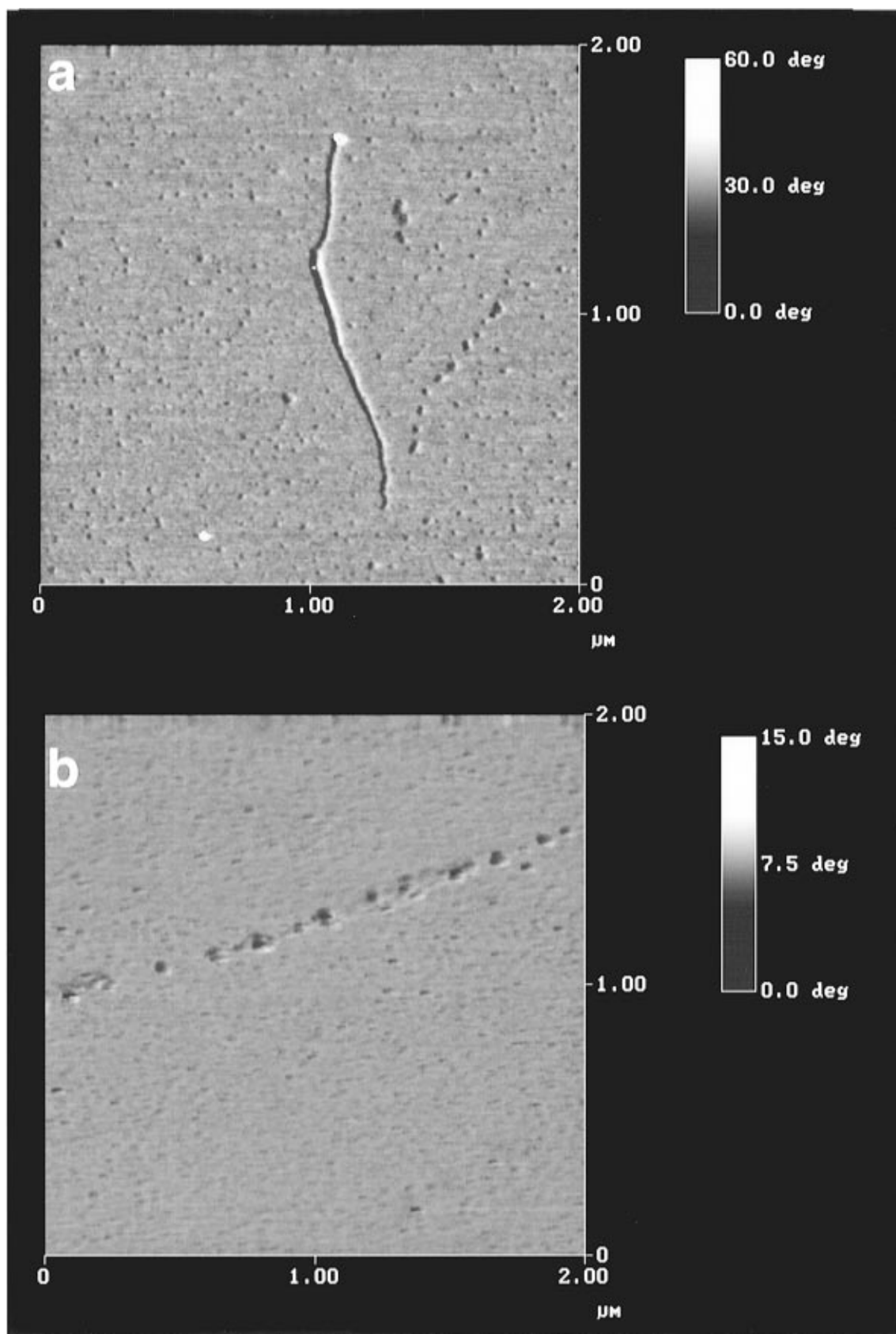
Figure 2. (a) A 2 μm TMAFM phase image of a freshly prepared magnesium hydroxide sample heated at 100 °C for 15 min. (b) Another view of the same sample.

mol) of $MgCl_2 \cdot 6H_2O$ are dissolved in water and reacted with 44 mL of 2 N NH_4OH to a total volume of about 400 mL in a 600 mL beaker. The $Mg(OH)_2$ precipitate is allowed to settle and then decanted and washed with at least 4 volumes of water to remove excess ions. The fresh $Mg(OH)_2$ slurry, concentrated down to about 100 mL, is then added to the organic−LiF solution.

After about 20 min of stirring, 9.2 g (0.036 mol) of Ludox HS-30, a Na^+-stabilized 30% silica sol (DuPont, now available from Aldrich) is added. The total volume is brought to about 500 mL, and the slurry is refluxed with stirring. Portions of the clay slurries were removed at various times, thoroughly washed, and kept wet before dilution for the AFM studies. All starting
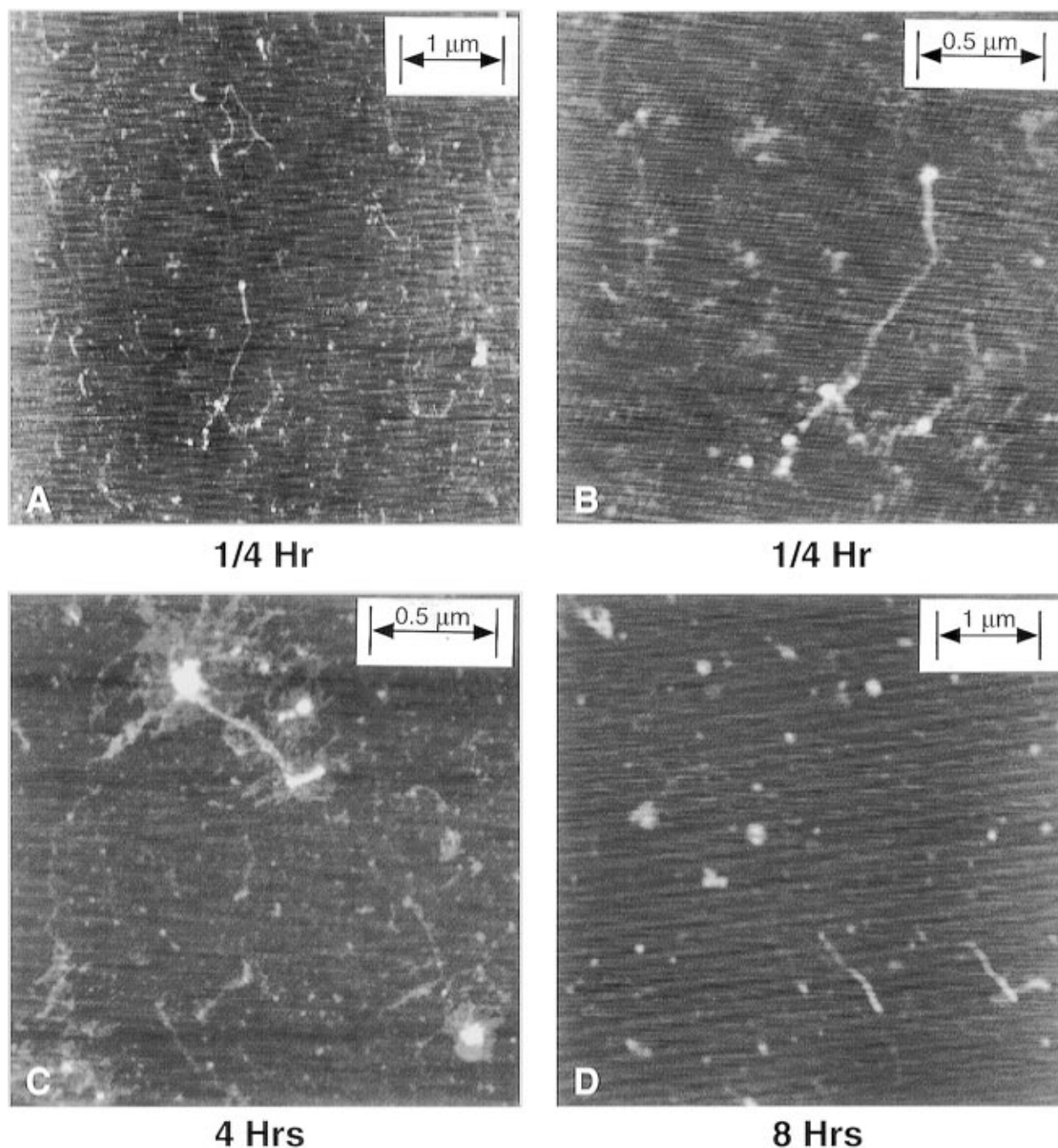
Figure 3. (a) A 5 μm TMAFM height image of the $^1/_4$ h refluxed sample. The interconnected stranded nature is apparent in the upper and lower central portions of the image; the contrast scale is 5 nm high. (b) A 2 μm height image of the $^1/_4$ h refluxed sample; this is a zoom of the lower central feature of Figure 2a. The spherical muclei appear interconnected by strands. The contrast is 5 nm high. (c) A 2 μm height image of the 4 h refluxed sample; three highly interconnected "globular cluster" features with multiple embedded nuclei are apparent. The contrast is 12 nm high. (d) A 5 μm height image of the 8 h refluxed sample; the image is dominated by ~100 nm lateral and ~1 nm height particles; the contrast is 6 nm high.

materials were obtained from Aldrich Chemical Co., Milwaukee, WI. A pure $Mg(OH)_2$ control sample was also prepared for AFM analysis.

Tapping Mode Atomic Force Microscopy (TMAFM). A Digital Instruments atomic force microscope (Nanoscope III) was utilized with the noncontact imaging technique referred to as "tapping mode". A 225 μm etched silicon (FESP) diving board

(14) (a) Carrado, K. A.; Thiyagarajan, P.; Elder, D. L. *Synthesis of Porous Materials: Zeolites, Clays, and Nanostructures;* Marcel Dekker: New York, Occelli, M. L., Kessler, H., Eds.; **1997**, 551. (b) Carrado, K. A.; Thiyagarajan, P.; Elder, D. L. *Clays Clay Miner.* **1996**, *44*, 506. (c) Carrado, K. A.; Forman, J. E.; Botto, R. E.; Winans, R. E. *Chem. Mater.* **1993**, *5*, 472. (d) Carrado, K. A. *Ind. Eng. Chem. Res.* **1992**, *31*, 1654. (e) Carrado, K. A.; Thiyagarajan, P.; Winans, R. E.; Botto, R. E. *Inorg. Chem.* **1991**, *30*, 794.

cantilever was utilized for low force constant (1–5 N/m). The nominal radius of curvature is approximately 5–10 nm. Resonant frequencies near the center frequency range of these cantilevers ~320–330 kHz were employed for imaging. The fresh solutions to be imaged were diluted with distilled water to a concentration of ~1 μg/mL for submonolayer coverage. Freshly cleaved mica was employed as a substrate and a ~100 μL drop was dispersed onto the surface and air-dried for 15–30 min and visually inspected with a 100× stereomicroscope for dispersion and characteristic clustering. A top viewing Nikon microscope with CCD camera and video monitor was employed once the sample was installed in the TMAFM for micropositioning of the cantilever over features of interest. Visual inspection of the dried dilute solutions at various times throughout the crystallization process, invariably revealed multi-micrometer clustering of
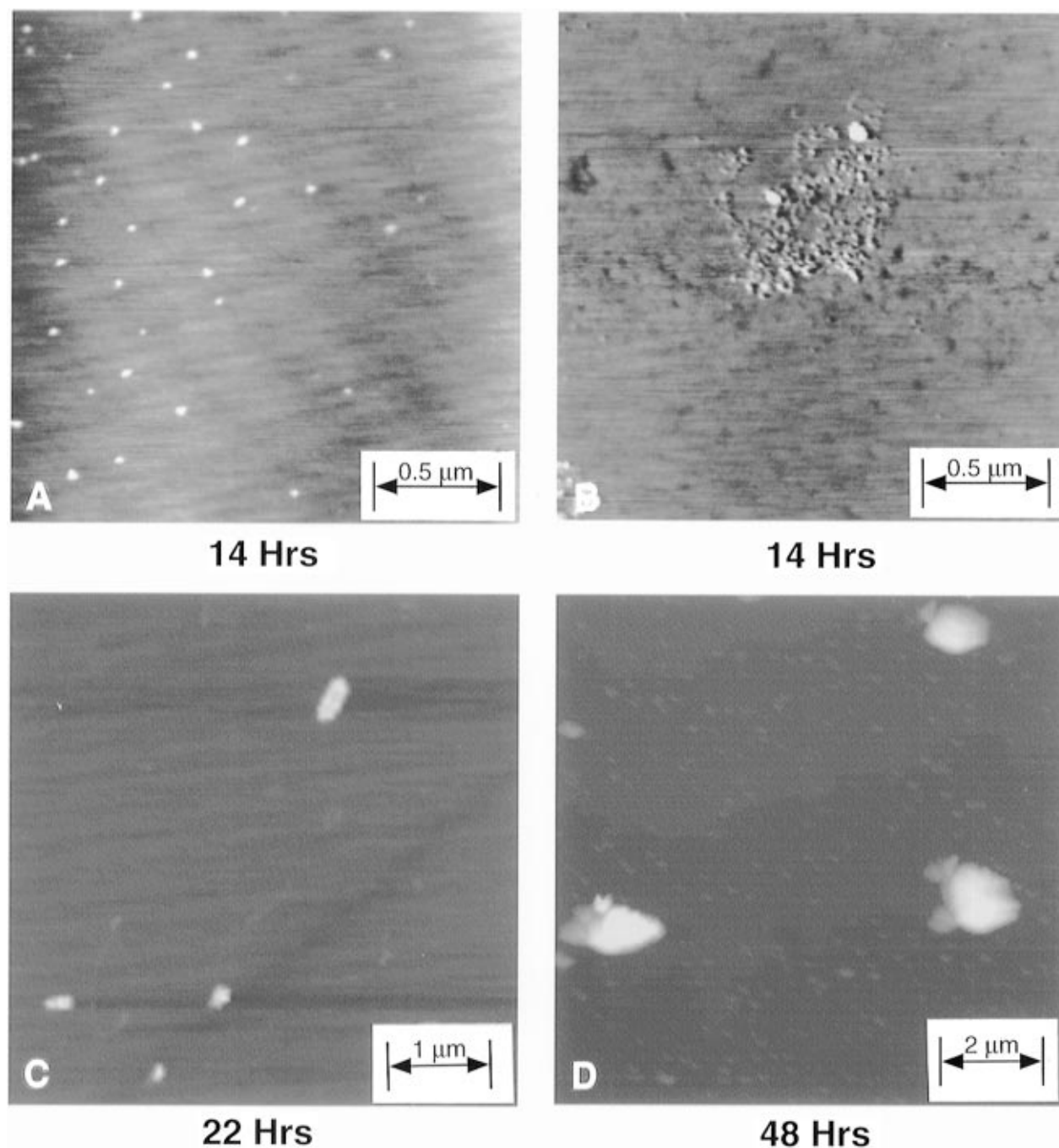
Figure 4. (a) A 2 μm height image of the 14 h refluxed sample. As observed in the 8 h sample, this view is dominated by ~100 nm lateral and ~1 nm height particles; the contrast is 12 nm high. (b) A 2 μm height image of the 14 h refluxed sample. The "globular cluster" appears as a disrupted network of aggregated particles. The contrast is 9 nm high. (c) A 5 μm height image of the 22 h refluxed sample. The individual hectorite clay particles have grown to several hundred nanometers laterally with greater heights (5−6 nm) than those previously observed. The contrast is 30 nm high. (d) A 10 μm height image of the 48 h refluxed sample, which is a common view of the large (1−2 μm) lateral and 100−200 nm height aggregated clay particles. The contrast is 1 μm high.

particulates and large regions between clusters which were chosen for imaging. Control samples of cleaved mica and cleaved mica with distilled water only, dried under identical conditions were imaged by optical and TMAFM microscopy. No indications of clustering were found in the control samples visually, and the TMAFM imaging revealed only large multi-micrometer planar regions free from nanophase materials. The cantilever was engaged and the feedback signal reduced until liftoff was achieved. The feedback setpoint was then reduced ~10% to reengage and achieve minimal force imaging to minimize disturbance of the hydrated soft protoclay samples. Stable imaging was routinely accomplished utilizing this engagement procedure and imaging conditions. Figures 1 and 2 display phase contrast images of the oscillating cantilever where slightly improved spatial resolution and contrast is observed. Figures

3 and 4 display height images where contrast is indicative of height; scales are indicated in the figure captions and on scale bars. Each image is representative of at least 10 views obtained for each sample.

Results

Figure 1 shows the TMAFM images of two of the major starting materials. The freshly prepared magnesium hydroxide used in the hectorite synthesis actually forms a colloidal suspension of brucite particles, which is in itself a layered mineral. The observed morphology of this in Figure 1a can be described as aggregates of smaller-sized (on the order of hundreds of angstroms) particles into a diffuse, random, loosely associated "jelly-like" network.

Table 1. Statistically Determined Particle Size Distributions from AFM Data for Synthetic TEA-Hectorites after Various Reaction Times[a]

time (h)	log mean height (nm)	geometric standard deviation[b]	% area	log mean length (nm)	geometric standard deviation[b]	% area
0.25	1.57 ± 0.05	1.43 ± 0.03	100	58.2 ± 1.5	1.33 ± 0.03	100
4	0.57 ± 0.03, 13.2 ± 2.20	1.46 ± 0.08, 1.47 ± 0.25	78, 22	111.7 ± 1.2	1.27 ± 0.01	100
8	0.38 ± 0.01, 0.84 ± 0.04	1.11 ± 0.01, 1.76 ± 0.06	47, 53	103.4 ± 0.4	1.21 ± 0.01	100
14	1.98 ± 0.05	1.22 ± 0.03	100	55.6 ± 0.3	1.11 ± 0.01	100
22	5.63 ± 0.07	1.31 ± 0.02	100	240 ± 4	1.35 ± 0.02	100
48	123 ± 7.00	1.68 ± 0.07	100	1321 ± 48	1.51 ± 0.05	100

[a] Reported errors are standard deviations in the curve fit approximations to a given parameter. [b] Geometric standard deviation = height or length corresponding to 84.13% probability divided by the log mean height or length.

Note that the scale of this image is larger than those used for the clay features in the following images. The few bright spots that occur are very large (at least in height) aggregates. Figure 1b of the silica sol starting material shows exceptionally uniform spheres of about 40−60 nm in diameter. Both of these control samples were collected, treated, and prepared at room temperature. It was also of interest to examine the morphological features of especially the brucite at reaction temperature. As a result of this, Figure 2 shows two typical images of pure brucite heated for just 15 min. There is a dramatic change in morphology after this short amount of time to what appears to be strings and long chains of small, round particles ("strings of pearls"). A few of these remain after an hour (image not shown), but beyond that point the field of view is dominated by simple particulates. This behavior becomes important when analyzing the crystallizing hectorite, as discussed below.

Figure 3 shows progressive crystallization of hectorite clay with reaction times from $1/4$ to 8 h. Recall that in addition to SiO_2 and $Mg(OH)_2$, there is also now a small amount of LiF and TEA present in the reactive sol−gel. The pictures of Figure 1 change dramatically when this clay slurry has been heated for just 15 min. This is generally taken as our baseline sample since clay is not evident in either X-ray diffraction (XRD) or Fourier transform infrared (FTIR) spectroscopy.[4a] Both parts A and B of Figure 3 are for this sample, with a 5 μm view of a "strand of pearls" and a 2 μm close-up of this cluster. Notice the resemblance to the pure brucite views in Figure 2. Figure 3c, the clay slurry at 4 h, is an image of three units that could be termed "globular clusters". This term is chosen because visually they appear to be comprised of "clouds" of material in which there are isolated patches of bright spots that may be crystallizing clay nuclei. Figure 3d shows the sample after 8 h, which appears similar but with perhaps a few less strands.

Figure 4 is for the 14−48 h samples, the time region in which no starting materials are evident by XRD and FTIR studies. Parts A and B of Figure 4 show two different images for the 14 h sample. The "globular clusters" of earlier now appear to have their networks broken into smaller pieces, aggregated close together. In addition, there are small particles occurring in a random orientation. There are also, not shown, aggregates several hundred nanometers in size with each piece about 100 nm in dimension. The 22 h sample shown in Figure 4c has bright spots on isolated particles that indicate high stacks of clay layers, since the brightness in these images is related to height. The 48 h sample in Figure 4d is a large field of view (10 μm) because this material is composed of very large aggregates in a field of smaller particles.

Particle size distributions were constructed by grouping visually measured length and height values into logarithmically evenly-spaced bins ranging from 0.17 to 10 000 nm in both length and height, with 10 bins per factor of 10 change in dimension. These distributions were fit with one or two cumulative log-normal distributions as defined by eq 1 (using the commercially available program PeakFit (Jandel Scientific)):

$$F_{LN}(x) = \sum_{i=1}^{n} 0.5 \left[1 + \text{erf}\left(\frac{[\ln(x/\bar{x_i})]}{[2^{0.5} \ln(\sigma_i)]} \right) \right] \quad (1)$$

In eq 1, x is a given length or height, $F_{LN}(x)$ is the cumulative log-normal probability density function, $\bar{x_i}$ is the log-mean length or height for the ith log-normal contribution, and σ_i is the geometric standard deviation in the length or height for the ith log-normal contribution.[15] The number of log-normal contributions, n, is either one or two, depending on whether or not the distribution is bimodal. From eq 1, one can show that the geometric standard deviation is equal to the length or height corresponding to a cumulative probability of 0.8413 divided by the log-mean length or height of the ith contribution. Granqvist and Buhrman[15] have shown that eq 1 can be derived from particle coalescence theory, which is valid for all but the narrowest particle size distributions ($\sigma < 1.2$).

The use of two log-normal distributions to describe the data was avoided except when clearly statistically justified. In no cases did the lengths require two log-normal distribution contributions. However, the particle heights after 4 h, and to a lesser degree after 8 h, did require two log-normal contributions. The log means, geometric standard deviations, and area percentages (for materials requiring two log-normal contributions) are summarized in Table 1. The errors reported in Table 1 are standard deviations in the curve fit approximations to a given parameter and should not be confused with the actual errors in the particle size measurements. Figure 5 displays the lengths and heights of individual particles (particle correlations) parametric in time.

Discussion

Smectite clays are known as 2:1 layer silicates because two tetrahedral silicate sheets sandwich a central metal-containing octahedral hydroxyl sheet in a single clay sandwich layer. Oxygen atoms at the tips of the tetrahedra in the silicate sheets point inward and replace two-thirds of the hydroxyls in the octahedral sheet.[16] In hectorite, the octahedral metal is primarily magnesium. There is some substitution by lithium ions (Li(I) for Mg(II)) which imparts a net negative charge to the layers. In this synthetic hectorite, the negative charge is approximately 0.6 per unit cell. The negatively charged layers are held together by interlayer cations (TEA in this case) and water molecules.

(15) Granqvist, C. G.; Buhrman, R. A. *J. Appl. Phys.* **1976**, *47*, 2200.
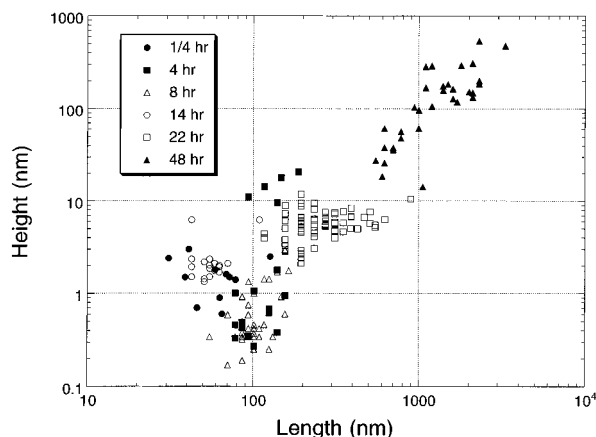(16) Grim, R. E. *Clay Mineralogy*; McGraw-Hill: New York, 1968; p 77.

Figure 5. A log−log plot of particle correlation using length and height values measured from images of several particles for each sample. The samples are crystallizing synthetic hectorite clays heated for various times as indicated on the plot.

Natural clay formation has recently been considered a reassembly of units derived from rock weathering.[17b] This involves a crystallization from supersaturated solutions that are in continuous supply from feldspar degradation. Specifically, silicic acid and metal ions build up clay crystals through polycondensation reactions.[7] This has been also considered a "self-assembly" process. It is assumed that a mixture of products occur in this way but, under the correct levels of supersaturation, any chaotic tangles of inorganic polymers formed will again dissolve and well-made, orderly, low-energy arrangements will persist. Appropriate levels of supersaturation are obviously common in nature under this view, allowing clay crystals to build from suitable nuclei. It is a geologically slow process that takes place near the Earth's surface near ordinary temperatures and pressures. As mentioned in the Introduction, laboratory clay synthesis conditions range widely from one type to another. Whether or not the supersaturation theory applies under these laboratory conditions is open to debate.

A vast array of clay microstructures exists. The different crystalline characters become quite evident under the electron microscope: plates, tubes, stacks, leaves, fibrils, scrolls, etc.[17] For example, kaolinite crystallizes in either plates or stacks as large hexagonal sheets, micas can form macroscopically large crystals, palygorskite and attapulgite have fibrous textures, while smectites are comprised of a "cornflakes" morphology—the small, thin flexible plates join together and curl at the edges.[18] Smectites are probably the most difficult to study by microscopic techniques because the particles sizes are so small (<2 μm) and are often comprised of many smaller aggregates; this has even been observed recently by AFM.[9c] Yet, since smectites form such an important class of materials commercially, it was decided to start with them for our initial AFM crystallization studies. The hectorite system is also convenient because this magnesium silicate crystallizes fairly quickly (2 days) using mild temperatures (100 °C).

A previous examination concerning the crystallization of the organohectorite clay system has employed the techniques of X-ray powder diffraction (XRD), FTIR, and thermal analysis.[4a] The samples studied were the dried products from aliquots taken during the synthesis at various times. Aliquots taken at the same time intervals were used for this AFM study but were left wet until dilution, and drying occurred on the sample mount. In this way, samples were hoped to have been as similar to those previously examined as possible. The major results of these previous studies were that (1) starting materials were evident for the first 8−14 h only, disappearing at some point between these times, (2) no clay products were evident at $^1/_4$ h but were just discernible at 4 h, and (3) further reaction time served to increase the crystallinity as seen by XRD. Another pertinent finding concerns this clay synthesis carried out at room temperature rather than at 100 °C.[4a] At room temperature and without TEA present, the purely lithium form of this hectorite takes 14 weeks to crystallize. With TEA present, there is a phase separation that occurs upon formation of an unidentified impurity phase and clay does not form at all.

The results of a previous small angle neutron scattering (SANS) study of organohectorite clay formation may also be relevant here.[14e] SANS profiles of the solutions only before and after complete reaction (0 and 48 h) were taken, so this was not a detailed time study. However, SANS results of the separate components may be revealing. In particular, the typical pure silica scattering profile was disturbed into a random network when the cation (in this case a porphyrin) was added. Such an addition had no effect on the scattering of the magnesium hydroxide.

Finally, it is appropriate here to compare recent microscopic results obtained for zeolite crystallization. One study has compared XRD crystallinity with scanning electron microscopy (SEM) observations;[19] SEM is possible for zeolites because single crystals often form to micrometer size. Amorphous microparticles were observed to form $1-6$ μm sized agglomerates, which then quickly crystallized to Na-X zeolite without any appreciable change in size. Uniform growth of crystal size was not observed by SEM. In another study, zeolite precursors were imaged by cryo-TEM (transmission electron microscopy) and also analyzed by small angle X-ray scattering.[20] These researchers labeled the zeolite precursors imaged by TEM as 5 nm diameter "globular structural units", which act to transfer silica and alumina from solution to the solid phase. In their scheme, the globular structural units consist of several "tetrapods" (segments of the final crystalline templated zeolite) that fuse to produce cylindrical bodies that constitute the final unit cell of this ZSM-5 zeolite. In this case, some crystal growth was apparent (from 5 to 80 nm).

It has been generally assumed in the case of synthetic hectorite that soluble silicate units condense on "pre-existing brucitic sheets",[14e] although this does not agree with the view taken of natural clay formation via polycondensation of species in supersaturated solutions. The AFM data indicate that the brucite particles are definitely involved in some way. The views of heated, pure $Mg(OH)_2$ are most telling. The morphologies are quite similar to what is seen in the $^1/_4$ h clay sample, although even here a degree of association is indicated in the clay precursor that is not present in the pure brucite. The individual strands of pure brucite appear to associate when the other components of a clay gel are present, and then the clay crystallization grows from there into rather spectacular morphologies (see the 4 h sample in Figure 3c for example). The AFM data indicate that the globular

(17) (a) Murray, H. H. *Appl. Clay Sci.* **1991**, *5*, 379. (b) Cairns-Smith, A. G.; Hartman, H. *Clay Minerals and the Origin of Life*; Cambridge Press: Cambridge, **1988**; Chapter 1.

(18) (a) Sudo, T.; Shimoda, S.; Yotsumoto, H.; Ata, S. *Electron Micrographs of Clay Minerals*; Elsevier: New York, 1981. (b) Bennet, R. H.; Bryans, W. R.; Hulbert, M. H. *Microstructure of Fine Grained Sediments*; Springer: New York, 1991.

(19) Shigemoto, N.; Sigiyama, S.; Hayashi, H.; Miyaura, K. *J. Mater. Sci. Lett.* **1994**, *13*, 660.

(20) Regev, O.; Cohen, Y.; Kehat, E.; Talmon, Y. *Zeolites* **1994**, *14*, 314.

clusters consisting of "strings of pearls" appear to behave more like the zeolite cases reported above. In this view, a globular cluster may consist of several clay precursor nuclei, which grow slightly to form clay units of a particular size that are then closely associated. Such a view would also agree with the results obtained for the hydrothermal synthesis of two smectites, montmorillonite[21] and beidellite,[22] from glass. In these cases, XRD shows that the size and thickness of a two-dimensional flake of smectite do not increase with increasing synthesis time, but rather an increase in the number of flakes occurs. The fact that crystal size does not increase with time means that an Ostwald ripening mechanism is not evident. In fact, the crystal size of natural samples is always so small that XRD profiles are broadened. A conclusion is made for montmorillonite, which is very similar to hectorite, that the fine particle size is probably not time-dependent but instead related to the "intrinsic nature of this material".[20]

If Ostwald ripening occurs, it is at the stage where the small clay "nuclei" are closely associated in the globular cluster. Extremely narrow particle size distributions of $\sigma \leq 1.2$ (the geometric standard deviations in Table 1, length data) are evidence of Ostwald ripening.[15] Broader distributions of $1.2 \leq \sigma \leq 1.5$ are, on the other hand, consistent with coalescence theory. Ostwald ripening is apparent in this system in the 8 and 14 h time frames. For example, at 14 h, a large collection of 25 nm spheres occurs in a small 700×700 nm area (see Figure 4b). These may have been growing since the clay precursor nuclei stage ("strings of pearls") but can grow only to about 80 nm in size until they have coalesced with each other (22 h). Beyond this point, there is no clear Ostwald ripening event. Any Ostwald ripening trends would also be observed in Table 1 and Figure 5. If such a scenario took place, the lateral dimension would grow with the height remaining constant, reflecting the increase in aspect ratio expected for larger and larger clay crystallites as they are allowed to grow. This is not generally the case, however. The significant rise in both values for the 48 h sample is simply due to the aggregation of smaller particles.

Figure 5 displays the lengths and heights of individual particles as a function of time. At a given time, the particle lengths are always unimodal. However, most noticeably at 4 h but still at 8 h, the heights of individual particles are distinctly bimodal. During this time, nucleation of the clay crystallites is occurring. Between 8 and 14 h, the nucleation is complete, as evidenced by the unimodal distribution of lengths and heights in the 14 h sample. At times longer than 14 h, particles appear to coalesce, as shown previously in Figure 4, and form substantially larger particles. The correlation between particle lengths and heights at longer times provides further evidence of a coalescence growth model, which is a critical finding for this system.

A discussion of the height images in terms of their contrast is also appropriate at this time. The contrast goes from darkest on the mica sample stage surface to very bright at the top surfaces of the particles imaged. The contrast bar is in the range of 5−12 nm high for the time frame of $^1/_4$ to 14 h, which means that the heights are fairly comparable throughout this time span. Beyond this point the proposed aggregation would indicate large particles, and in fact the contrast heights go from 30 nm at 22 h all the way to 1 μm at 48 h. One flat clay sheet is only 1 nm high, and the *d*-spacing of TEA-hectorite is about 1.5 nm, which reflects an interlayer distance of 0.5 nm. A height of 5−12 nm means that a few layers are allowed to build up on each other before aggregation occurs.

Conclusions

This is the first time that temporal snapshots of a clay's nucleation and crystallization processes have been presented. The view is extremely interesting and does not support the expectation of small crystallites slowly ripening into larger plates by Ostwald ripening. Instead, larger aggregates appear to coalesce from numerous small crystallites that are closely associated in globular networks similar in appearance to "strings of pearls" at the initial stages of crystallization. The evidence for direct magnesium hydroxide layer participation at the earliest nucleation stages is clear. Detailed ^{13}C NMR solution studies are also beginning to complement these results at very early reaction times.[23]

Future work will attempt to probe the globular clusters in the initial stages as they exist in solution, since in the current study the gelatinous, swollen entities were dried out. This can still be attempted by TMAFM, in conjunction with attempts to image a single "pearl", or clay nucleation site. An in situ study of the crystallization would be especially interesting. Future studies will also concentrate on obtaining high-resolution images of the formed clay species to determine when the hexagonal silicate layer structure become evident.

(21) Nakazawa, H.; Yamada, H.; Yoshioka, K.; Adachi, M.; Fujita, T. *Clay Sci.* **1991**, *8*, 59.
(22) Yamada, H.; Yoshioka, K.; Nakazawa, H. *Miner. J.* **1991**, *7*, 300.

(23) Song, K.; Botto, R. E.; Gregory, D.; Carrado, K. A. Manuscript in preparation.